Effect of Segmental Configuration on Properties of *n*-Propyl-Bridged Polycyanurate Networks

Andrew J. Guenthner,*,† Benjamin G. Harvey,§ Andrew P. Chafin,§ Matthew C. Davis,§ Jacob J. Zavala,‡ Kevin R. Lamison,‡ Josiah T. Reams,‡ Kamran B. Ghiassi,† and Joseph M. Mabry†

†Aerospace Systems Directorate and ‡ERC Incorporated, Air Force Research Laboratory, Edwards AFB, California 93524, United States

§Weapons Division, Naval Air Warfare Center, China Lake, California 93555, United States

Ⓢ *Supporting Information*

ABSTRACT: The effect of the chemical configuration of network segments on the physical properties, cure properties, mechanical performance, and chemical stability of polycyanurate networks was investigated via synthesis, network formation, and characterization of an isomeric series of *n*-propyl-bridged cyanate ester monomers. Configurations that provide cyanurate oxygen atoms with either nearby methyl groups or nearby bridge groups exhibited decreased moisture uptake by up to 50%, along with a roughly 20−40 °C reduction in the loss in glass transition temperatures due to hydrolysis, for networks immersed in 85 °C water for 96 h. In *ortho,para*-linked aryl cyanates, dry glass transition temperatures of cured networks were reduced compared to analogous *para,para*-linked networks by only about 10 °C, compared to a reduction of 30 °C in *ortho*-methylated cyanate ester networks, leading to higher "wet" glass transition temperatures in the *ortho,para*-linked networks. Neither methyl groups nor bridge groups in a position *ortho* to the reactive cyanate ester groups prevented the creation of networks with >99% conversion at cure temperatures of 230 °C. Networks with placement of methyl groups in a position *ortho* to the cyanate ester exhibited char yields in nitrogen at 600 °C of 46−47% compared to 43% for networks with methyl groups in the corresponding *meta* position, regardless of whether a sterically hindered environment was present around the cyanurate oxygen. These results illustrate the manner in which the chemical configuration around reactive groups can substantially modify the properties of networks even when the number density and type of reactive group present do not change.
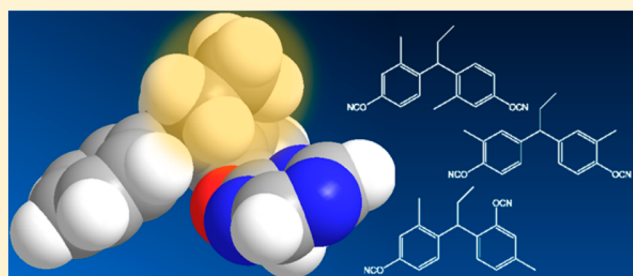
INTRODUCTION

As a class of thermosetting polymer networks, polycyanurates[1−4] have proven to be exceptionally useful in extreme environments due to the highly stable nature of the cyanurate cross-links formed from cyanate ester monomers. Some notable environments where polycyanurate networks have proven useful include the charged particle and radiation environment around Jupiter encountered by the Juno space probe,[5] the heat of atmospheric entry for the Mars Curiosity heat shield,[6] and the intense neutron bombardment expected within the ITER thermonuclear fusion reactor[7−9] and other superconducting magnets exposed to high radiation doses.[10] From a more fundamental perspective, the high stability of the cyanurate cross-link allows for the formation of networks with a very well-defined[11] and, fortuitously, easy to monitor chemical structure even in the fully cross-linked state. This feature, along with the simplicity of network formation by straightforward heating of the monomer with very little net shrinkage or volatile generation, makes polycyanurate networks ideal candidates for studying the general physics of highly cross-linked polymer networks and establishing useful structure−property relationships.

An important prerequisite for developing structure−property relationships is the availability of a variety of carefully controlled and varied chemical structures, with quantifiable structural characteristics. Careful control of the chemical structure enables the avoidance of problems such as a network with too high of a glass transition temperature (T_G) at full cure. Such networks typically cannot be cured completely without chemical degradation due to the high cure temperatures required, thus making it impossible to measure the properties of the fully cross-linked structure.[12] At the same time, large variations in structure must also be achievable; otherwise, the structure−property correlations are likely to become unduly biased by a specific subset of chemical features appearing in all the structures.

Recently, bio-based materials such as anethole,[13,14] resveratrol,[15,16] eugenol,[17,18] cresol,[19] vanillin,[20] and turpentine[21] have been utilized to synthesize cyanate ester and other high-temperature network[22−30] monomers with a much wider variety of chemical structures than found in the typical

petroleum-derived bisphenol or novolac monomers. The wider variety of structures has facilitated systematic structural comparisons, such as the effect of a methoxy group *ortho* to the cyanate ester group, on the properties of networks.[31] With cresol-based monomers in particular, the bridge type, cyanate ester configuration, and methyl group configuration in a bis-phenyl motif may all be varied systematically. Figure 1 illustrates this concept using four isomeric chemical structures.
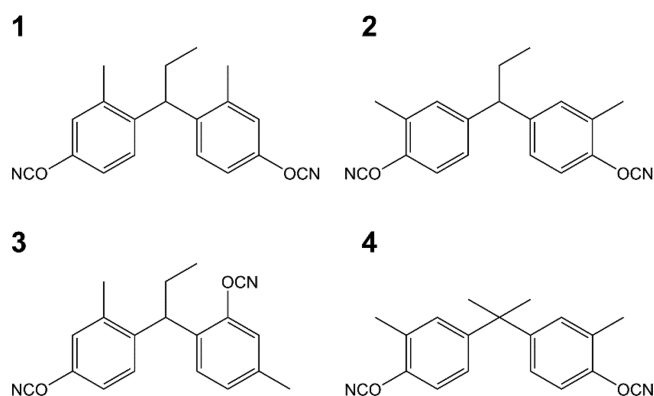
Figure 1. Illustration of a set of four isomeric bis(cyanate ester) monomeric compounds derived from *m*-cresol (**1** and **3**) or *o*-cresol (**2** and **4**) in which the methyl group configuration (compare **1** and **2**), cyanate ester configuration (compare **1** and **3**), and bridge group (compare **2** and **4**) are all varied. Note that some properties for **1** prepared from creosol and its networks[31] as well as **4** and its networks[32] have been previously published.

Previous studies of polycyanurate networks have revealed that methyl group configuration can have a significant impact on key physical properties of polycyanurate networks, such as moisture uptake.[32,33] In particular, steric hindrance around the cyanate ester group is believed to reduce moisture uptake, although it may also interfere with cure chemistry. Because the cure reactions for cyanate ester monomers may be initiated with a proton source, and because of the ability for protons to fit easily into spaces where water molecules do not fit, it should be possible to identify forms of steric hindrance that prevent water uptake without unduly sacrificing ease of cure. One very interesting such candidate is the use of an *ortho,para*-linked cyanate ester configuration in a bis-phenyl monomer with a substantial bridge group. As shown in Figure 2, in this configuration, the bridge itself may provide some additional steric hindrance around the cyanate ester group *ortho* to the bridge linkage. The *ortho,para*-linked monomers are typical side products of *para,para*-linked monomer synthesis. In particular, when *m*-cresol is used as a starting material, the formation of the *ortho,para*-linked monomer may be enhanced by steric effects. If these *ortho,para*-linked structures were to impart a useful property such as lower moisture uptake, then it may be possible to produce superior networks from a broader variety of starting materials, with less demanding synthesis and purification requirements.

In this paper, we report on a systematic study of *n*-propyl-bridged, bis-phenyl cyanate ester monomers that can be derived from bio-based starting ingredients. The *n*-propyl bridge is large enough to contribute to steric hindrance, while simultaneously lowering the glass transition temperature of the network at full cure sufficiently to avoid issues with degradation, but not so large as to unduly compromise thermal and mechanical performance. We show that the use of the *ortho,para*-substituted monomer is effective at lowering moisture uptake while preserving other key properties. Through this carefully selected systematic study, we therefore validate a key general principle for minimizing moisture uptake in densely cross-linked polymer networks.

■ EXPERIMENTAL SECTION

Materials. Reagents and solvents were obtained commercially and used as received unless otherwise specified.

General Considerations. ^{1}H and ^{13}C NMR data were obtained on a Bruker Avance II 300 MHz spectrometer (^{1}H at 300 MHz, ^{13}C at 75 MHz) using CDCl3, acetone-d_6, or DMSO-d_6 and spectra referenced against residual solvent or tetramethylsilane. Spectra are available in the Supporting Information. Mass spectral data were obtained on an Agilent 6890/5973N gas chromatograph system (details in the Supporting Information). Elemental analysis was conducted by Atlantic Microlab, Inc. (Norcross, GA).

Monomer Synthesis. *4,4′-(Propane-1,1-diyl)bis(3-methylphenol) (5) and 2-(1-(4-Hydroxy-2-methylphenyl)propyl)-5-methylpheol (7).* A mechanically stirred mixture of 144 mL of propionaldehyde (2 mol) and 840 mL of *m*-cresol (8 mol) was cooled to −10 °C while 4 mL of concentrated HCl was added over 30 min. After an additional 30 min the cooling bath was removed, and the mixture was stirred for 2 h. Excess *m*-cresol was then removed by heating the mixture under high vacuum (0.3 Torr) until the internal
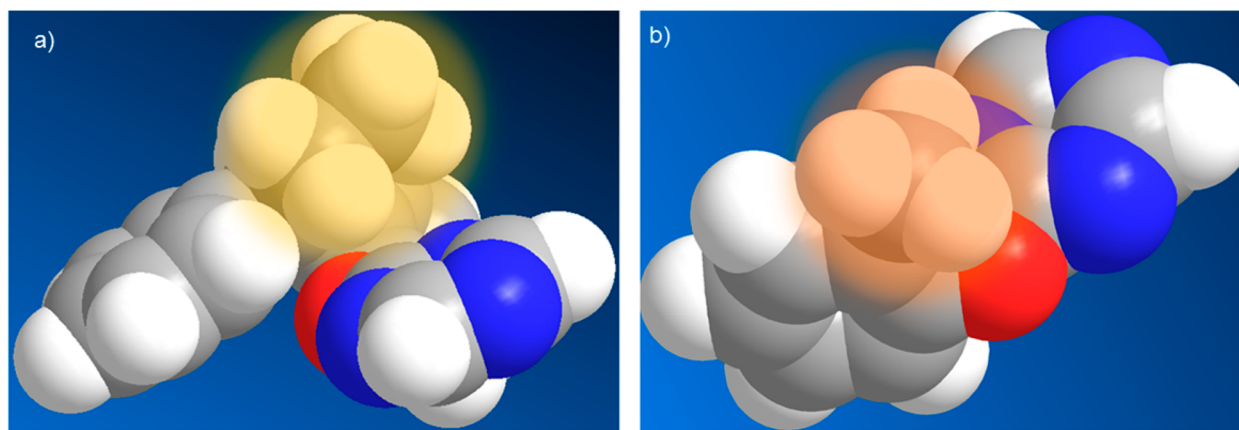
Figure 2. Illustration of various forms of steric hindrance found in the repeat structures of polycyanurate networks: (a) a bulky bridge group (highlighted yellow) may hinder access to a cyanurate oxygen atom in a manner similar to (b) a methyl group (highlighted orange) *ortho* to a cyanurate linkage. Color scheme, C: gray; H: white; N: blue; O: red. For simplicity, repeat unit structures are H-terminated.

temperature rose above 90 °C. The residue was taken up in a solution of 240 g of NaOH in 500 mL of water. This was added to a mixture of 600 mL of concentrated HCl and ice. This mixture was extracted with 1.5 L of ether. The extract was washed with water and then dried (MgSO$_4$) and concentrated under reduced pressure to give 526.95 g of a brown glass (100%). This was determined to be 10% of the *ortho-,ortho*-isomer, 47% of the *ortho-,para*-isomer, 36% of the *para-,para*- isomer, and about 6% trimers. Three successive recrystallizations from hot toluene provided pure 4,4′-(propane-1,1-diyl)bis(3-methylphenol) (**5**) in an overall yield of 9%. The filtrate from the recrystallizations was allowed to stand for several days upon which crystals of 2-(1-(4-hydroxy-2-methylphenyl)propyl)-5-methyl-phenol (**7**) separated from the mixture and were collected. Bisphenol **5** was spectroscopically identical to a previous report.[31] Bisphenol **7** was obtained as a white powder; mp 120−125 °C. ^{1}H NMR (acetone-d_6): 8.1 (s, 1H), 7.9 (s, 1H), 7.12 (d, 1H), 6.86 (d, 1H), 6.61 (m, 4H), 4.35 (t, 1H), 2.19 (s, 3H), 2.16 (s, 3H), 1.9 (m, 2H), 0.88 (t, 3H). ^{13}C NMR (acetone-d_6): 154.96, 154.45, 137.74, 135.79, 134.03, 129.01, 127.83, 127.56, 120.15, 116.87, 115.44, 112.23, 39.53, 20.08, 18.94, 12.11.

4,4′-(Propane-1,1-diyl)bis(1-cyanato-3-methylbenzene) (1). A mixture of **5** (23.17 g, 90.4 mmol) and cyanogen bromide (20.11 g, 0.190 mol, 2.1 equiv) in 300 mL of THF was cooled to −30 °C while triethylamine (28 mL, 0.201 mol, 2.2 equiv) was added dropwise. The mixture was allowed to warm to room temperature and stirred for 30 min then washed with 300 mL of brine, dried with MgSO$_4$, and concentrated under reduced pressure to give 32.89 g of a tan liquid. This was chromatographed on silica gel using 15% ethyl acetate/hexanes to give 22.78 g of a clear liquid (82%). A single peak was observed in the GC/MS chromatogram, and the NMR data was identical to that from a previous report.[31]

1,1-Bis(4-hydroxy-3-methylphenyl)propane (6). A round-bottom flask equipped with magnetic stir bar was charged with *o*-cresol (20 g, 185 mmol, 2 equiv), H$_2$O (40 mL), and propionaldehyde (5.2 g, 90 mmol). The mixture was cooled in an ice bath while a 48% aqueous HBr solution (40 mL, 237 mmol) was added dropwise over 1.5 h. Once the addition was complete, the cooling bath was removed, and the mixture was stirred at room temperature for 48 h. Afterward, the mixture was partitioned between Et$_2$O (300 mL) and H$_2$O (300 mL). The organic layer was washed again with H$_2$O (300 mL) and then brine (300 mL), dried over MgSO$_4$, and filtered. The solvent was removed under reduced pressure, and the remaining oil was fractionally distilled at 1 Torr. The excess *o*-cresol distilled first, followed by the bisphenol as a thick, pale yellow oil. The crude bisphenol was recrystallized from cyclohexane to give the product as colorless needles; mp 85−87 °C [lit. 94 °C].[34] ^{1}H NMR (DMSO-d_6): 8.97 (s, OH), 6.89 (d, *J* = 1.7 Hz, 2H), 6.84 (dd, *J* = 8.4 and 2.3 Hz, 2H), 6.65 (d, *J* = 8.2 Hz, 2H), 3.47 (t, *J* = 7.7 Hz, 1H), 2.06 (s, 6H), 1.88 (pent, *J* = 7.1 Hz, 2H), 0.77 (t, *J* = 7.1 Hz, 3H). ^{13}C NMR (DMSO-d_6): 153.24, 136.06, 129.66, 125.32, 123.27, 114.31, 51.03, 28.25, 16.09, 12.81. Anal. Calcd for C$_{17}$H$_{20}$O$_2$: C, 79.65; H, 7.86. Found: C, 78.90 ; H, 7.87.

1,1-Bis(4-cyanato-3-methylphenyl)propane (2). **6** (1.35 g, 5.27 mmol) was dissolved in acetone (15 mL). The mixture was then cooled and stirred in a −20 °C bath. Next, cyanogen bromide (1.6 g, 15.8 mmol, 3 equiv) was added to the mixture in one portion and allowed to dissolve completely. Triethylamine (1.2 g, 11.9 mmol, 2.2 equiv) was then added dropwise over 30 min with the aid of an addition funnel. Shortly after the addition was started, a white precipitate formed. Afterward, the mixture was stirred at ambient temperature for 1.5 h. The reaction was partitioned between Et$_2$O (25 mL) and H$_2$O (50 mL). The organic layer was separated and washed with H$_2$O (2 × 50 mL) and then with brine (50 mL). The organic layer was separated, dried over MgSO$_4$, and filtered, and the solvent was then removed under reduced pressure, leaving a colorless oil. The oil was stored under vacuum and eventually began to crystallize. The crude solid was slurried with isopropyl alcohol (15 mL) and filtered on a medium porosity glass fritted filter funnel. Further purification by recrystallization from heptane gave the product as colorless needles (840 mg, 50%); mp 95−97 °C. ^{1}H NMR (CDCl$_3$): 7.35 (d, *J* = 8.5

Hz, 2H), 7.13 (dd, *J* = 8.5 and 2.3 Hz, 2H), 7.06 (d, *J* = 2.1 Hz, 2H), 3.76 (t, *J* = 7.7 Hz, 2H), 2.28 (s, 6H), 2.04 (m, *J* = 7.4 Hz, 2H), 0.9 (t, *J* = 7.4 Hz, 3H). ^{13}C NMR (CDCl$_3$): 149.68, 142.84, 131.07, 126.35, 126.05, 114.23, 108.76, 51.23, 28.07, 15.08, 12.17. GC-MS (EI) *m/z*: 306.1 [M] Anal. Calcd for C$_{19}$H$_{18}$N$_2$O$_2$: C, 74.49; H, 5.92; N, 9.14. Found: C, 74.22; H, 6.13; N. 9.07.

2-Cyanato-1-(1-(4-cyanato-2-methylphenyl)propyl)-4-methyl-benzene: (3). A mixture of **7** (15.05 g, 59 mmol) and cyanogen bromide (13.06 g, 123 mmol, 2.1 equiv) in 250 mL of THF was cooled to −30 °C, and triethylamine (18 mL, 129 mmol, 2.2 equiv) was added dropwise. The mixture was allowed to warm to ambient temperature, stirred for 30 min, and then washed with 250 mL of brine. The organic layer was dried with MgSO$_4$ and then concentrated under vacuum to give 18.75 g of an orange oil. This was chromatographed on silica gel using 15% EtOAc/hexanes to give 10.01 g of a clear liquid (55%). ^{1}H NMR (acetone-d_6): 7.15−7.43 (m, 6H), 4.38 (t, 1H), 2.37 (d, 6H), 2.04 (q, 2H), 0.92 (t, 3H). ^{13}C NMR (acetone-d_6): 151.22, 151.10, 140.62, 139.76, 139.20, 129.33, 129.16, 129.05, 127.96, 116.79, 114.95, 112.61, 108.69, 108.64, 40.11, 28.10, 20.04, 18.87, 11.71. GC-MS (EI) *m/z*: 306.1 [M]. Anal. Calcd for C$_{19}$H$_{18}$N$_2$O$_2$: C, 74.49; H, 5.92; N, 9.14. Found: C, 74.46; H, 6.03; N. 9.09.

Preparation of Networks. Prior to cure reactions, monomers were further purified by dissolution in dichloromethane, followed by passage through a W-Prep2XY Yamazen flash chromatography column, and removal of the solvent under reduced pressure. All monomers were first melted at 90−120 °C. The monomer was then either placed directly into a hermetically sealed differential scanning calorimetry (DSC) pan or degassed under 300 mmHg and poured into one or more silicone rubber molds having a disc-shaped cavity and cured using a predetermined time−temperature schedule under flowing nitrogen, then cooled, and demolded. The resultant discs measured approximately 12 mm in diameter by 4 mm thick.

Characterization Techniques for Networks. *Differential Scanning Calorimetry (DSC).* 5−10 mg pieces of cured networks were removed from a molded disc and hermetically sealed in an aluminum DSC pan. Samples were then ramped under 50 mL/min of flowing nitrogen at 10 °C/min, first heating to 350 °C, cooling to 100 °C, and then reheating to 350 °C, using a TA Instruments Q200 differential scanning calorimeter. Residual enthalpies of cure were determined based on an algorithm for generating baselines described in a previous publication.[32]

Thermogravimetric Analysis (TGA). Pieces of cured discs weighing approximately 5 mg were removed and placed in a TA Instruments Q5000 thermogravimetric analyzer. These samples were then heated to 600 °C, under nitrogen, and in separate experiments, in air, at 10 °C/min.

Oscillatory Thermomechanical Analysis (OTMA). Cured discs were also tested via oscillatory thermomechanical analysis (OTMA) with a TA Instruments Q400 series analyzer under 50 mL/min of nitrogen flow. The discs were initially held in place with a compressive force of 0.2 N using the standard ∼5 mm diameter flat cylindrical probe. The force was then modulated at 0.05 Hz over an amplitude of 0.1 N (with a mean force of 0.1 N), and the temperature was ramped twice (heating and cooling) between −50 and 200 °C (to aid in determination of thermal lag) followed by heating to 350 °C, cooling to 100 °C, and reheating to 350 °C, all at 50 °C/min. For samples previously exposed to hot water, the heating rate was decreased to 20 °C/min. The order of segments was as follows: heating to 350 °C, cooling to 100 °C, two cycles between 100 and 200 °C for thermal lag determination, and finally heating to 350 °C. The details of the thermal lag determination procedure have been reported previously.[32]

Infrared Spectroscopy. The cured discs were cut using a Struers rotary saw with a diamond blade to expose a fresh, smooth surface. Fourier transform infrared spectroscopy (FTIR) was carried out on these surfaces using a Thermo Scientific Nicolet 6700 spectrometer in attenuated total reflectance mode with the ZnSe crystal attachment. A total of 512 scans were completed on these surfaces with a resolution of 4 cm^{-1} to obtain spectra. Background values at 1850, 2700, and 3300 cm^{-1} were used to fit a quadratic global baseline. After

Table 1. Summary of DSC Data

monomer	$T_{G,monomer}$ (°C)	T_m (°C)	ΔH_m (kJ/mol)	ΔH_{cure} (J/g)	ΔH_{cure} (kJ/equiv)	$T_{cure\text{-}onset}$ (°C)	$T_{peak\text{-}cure}$ (°C)
1	-35 ± 1	n/a	n/a	714 ± 58	109 ± 9	276 ± 8	302 ± 3
2	n/a	99.1	39	717	110	271	303
3	-22 ± 1	62.6 ± 0.3	24 ± 1	710 ± 49	109 ± 8	298 ± 12	318 ± 6

subtracting the global baseline, the integrated area between 1480 and 1510 cm^{-1}, containing the aromatic peak near 1500 cm^{-1}, was used as a reference for normalization. After subtracting the global baseline, the integrated area between 2200 and 2300 cm^{-1} was calculated, and subtracted from a local secondary baseline between values at 2450 and 2150 cm^{-1}, to determine the peak area associated with residual cyanate ester groups.

Other Physical Characterization. Sample densities were determined using a Mettler-Toledo analytical balance with an attachment for specific gravity determination. Ethanol (ACS Reagent grade from Sigma-Aldrich) was used as the immersion medium, as it is superior to water for avoiding formation of bubbles adhered to the samples. A minimum of four weight measurements were collected and recorded per sample, making use of the cured discs prior to removal of portions for any other testing. For water immersion testing, cured discs were dried to a ± 0.0001 g constant weight in a vacuum desiccator, then weighed, and immersed in approximately 250 mL of deionized water maintained at 85 °C for 96 h. After removal from the water, samples were patted dry and weighed to determine the moisture uptake (on a dry weight basis).

■ RESULTS AND DISCUSSION

Monomer and Cure Characteristics. Note that a new batch of **1** was synthesized from *m*-cresol for use in this study; its properties match those previously reported[31] (see Supporting Information). Isomers **2** and **3** of **1** exhibit behavior typical of highly pure cyanate ester monomers. Key features of DSC data are listed in Table 1. Figure 3 shows the DSC trace
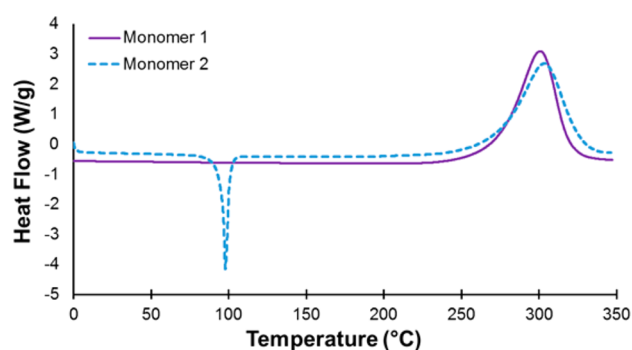
Figure 3. DSC (first heating) of **2** after purification by flash chromatography, compared to newly synthesized sample of non-crystalline **1** (after similar purification) for reference.

for **2** (uncured) compared to **1**. Although **1** is an extremely stable supercooled liquid, **2** crystallizes readily and thus exhibits a melting point just below 100 °C in the DSC trace. The cure characteristics of both are very similar, indicating that a similar level of monomer purity was attained. Because DSC cure characteristics are highly dependent on monomer purity, the effect of the chemical structural differences between **1** and **2** on cure characteristics is not reliably attainable from an analysis of the DSC data.

Figure 4 provides a DSC comparison on uncured **1** and **3**. Although a melting point for **3** was observed in some sample runs, a stable supercooled liquid was readily attainable under quiescent conditions in the DSC instrument. The cure
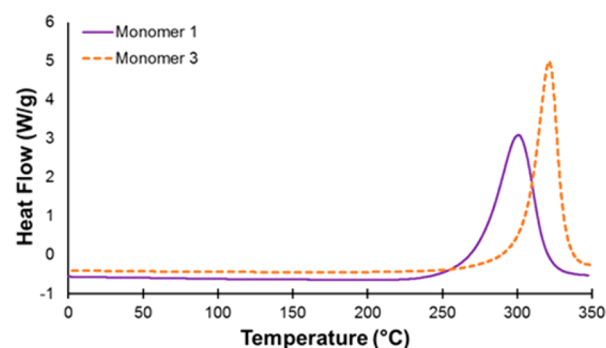
Figure 4. DSC (first heating) of **3** after purification by flash chromatography, compared to newly synthesized sample of **1** for reference.

exotherm for **3** occurs at higher temperatures than for **1**, possibly indicating that a lower level of catalytic impurities (such as phenol-containing compounds)[35] was obtained during chromatography of **3**. The impurity profile of **3** is important to consider during subsequent comparisons of the properties of networks derived from this compound.

Figure 5 shows the second heating scans of these (now cured) monomers. A very underappreciated aspect of the
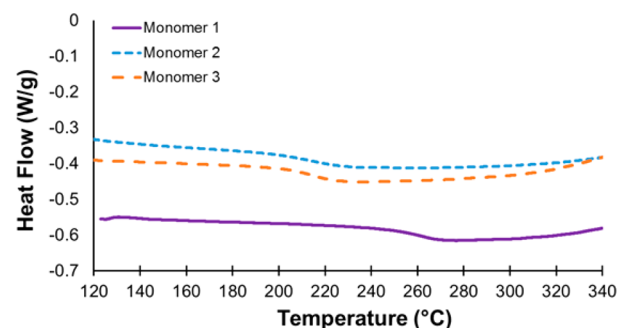
Figure 5. DSC (second heating) of **2** and **3** after purification by flash chromatography, compared to newly synthesized sample of **1** for reference. Note that the initial DSC heating results in cure temperatures in excess of 300 °C, which leads to some degradation and a T_G below the maximum possible value for the cured networks.

commonly performed analysis of DSC second heating scans for high-temperature thermosetting networks is that the vast majority of the cure that takes place during the first DSC scan involves temperatures (well over 250 °C in this case) that are significantly higher than those typically utilized to cure the networks without degradation (typically 150−200 °C for cyanate esters). Under these conditions, side reactions that destroy the reactive groups prior to network formation may be significant, leading to T_G values that are well below those achieved by completely curing the network more slowly at lower temperatures. Thus, a reliable inference from Figure 5 is that under typical cure conditions for polycyanurates, relatively stable networks with a T_G of over 200 °C may be formed from these monomers.

Network Characteristics. Conversion data for the networks after cure were derived from a maximum-likelihood statistical algorithm that combines DSC residual cure and T_G data, FTIR data, and the diBenedetto equation.[36] The method is detailed in the Supporting Information and enables measurement of conversions typically to a precision of better than 1%. This level of precision is important in establishing the structure−property relationships that are discussed below.

The weight gain data resulting from exposure to deionized water at 85 °C for 96 h for the cured networks is shown in Figure 6. Remarkably, despite the chemical similarity and nearly
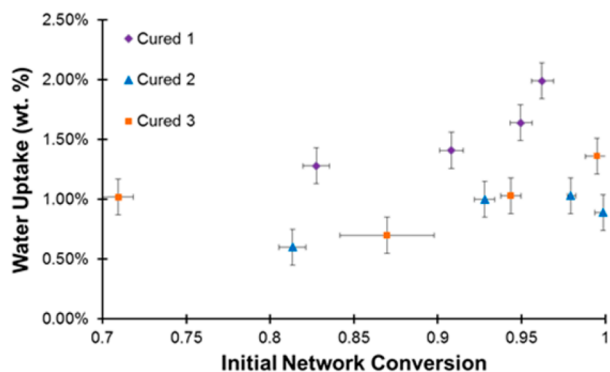

Figure 6. Water uptake after immersion for 96 h at 85 °C of cured networks.

identical density of favorable sites for water uptake in these networks (see Supporting Information for calculations), the observed weight gains differ by up to a factor of 4. Thus, the extent of water uptake appears to depend very substantially on the detailed physical structure of the network segments in the vicinity of these sites. In accord with previous studies on the effect of methylation *ortho* to cyanate ester groups on water uptake,[32,33] the presence of the methyl groups in network **2** results in a roughly 50% decrease in water uptake compared to network **1**, at all conversions examined. This effect has been attributed to steric hindrance of the cyanurate oxygen, which is a favored site for water uptake due to its polarity. Electronic effects caused by the *ortho* substitution of an aliphatic group near the cyanurate oxygen also may play some role.

Perhaps even more remarkably, network **3**, in which only one of the two cyanate ester groups has an *ortho* substituent, namely the bridge rather than a methyl group, exhibits nearly the same comparative decrease in water uptake as network **2**, in which both cyanate ester groups are *ortho* to methyl groups. Only when the effect of conversion on water uptake is considered does network **2** provide a clearly superior characteristic. In agreement with numerous previous studies,[32,37−40] the water uptake increases with increasing conversion above about 85% conversion but, where data are available, shows a decrease in uptake with increasing conversion below about 85% conversion. The former effect is suppressed in network **2**, as in previously studied *ortho*-methylated cyanate ester networks,[32] but only partly suppressed in network **3**. These differences reinforce the conclusion that moisture uptake is highly dependent on the physical and chemical environment around favored sites for water uptake.

A simple way of examining the characteristics of the networks in order to gain insight into how physical structure impacts properties such as moisture uptake is to calculate the packing fraction. These calculations (provided in Supporting Informa-

tion) were carried out with the aid of the correlations developed by Bicerano[41] and Georjon and Galy.[38] The results, shown in Figure 7, indicate that (despite some anomalous
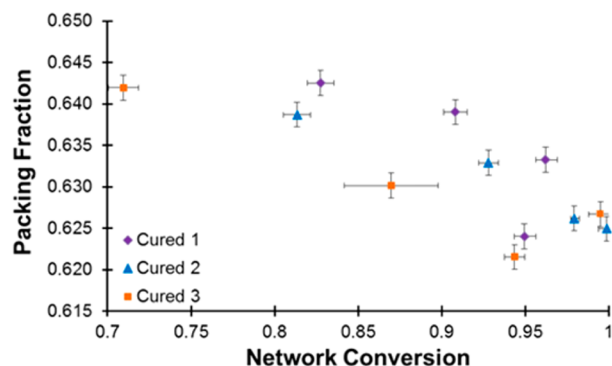

Figure 7. Packing fraction at 293 K of cured networks.

individual data points) the packing fraction is highest (and therefore free volume is lowest) in network **1**, with slightly more free volume in network **2** and considerably more in network **3**. As is typical for polycyanurate networks,[37,38] the free volume increases steadily as conversion increases, across the entire range of conversions studied.

Network **1**, with the highest packing fraction and lowest free volume, exhibits the highest water uptake. In fact, as seen with comparisons among other polycyanurate networks of varied chemical composition, there is no apparent correlation between overall free volume (at a given conversion) and moisture uptake.[42] Moisture uptake characteristics therefore appear to depend far more on local details of the structure near preferred sites for water uptake than on overall network physical properties. Nonetheless, as with previous comparative data among networks with different monomer chemical composition,[32,37,43] networks with lower glass transition temperatures at full cure exhibit characteristically lower moisture uptake. Whereas previous speculation about the mechanism underlying this correlation focused on differences in the density of favored sites for water uptake,[42] in the current work the density of these sites changes by less than 2% (see Supporting Information) at a given conversion.

In addition to slowing down hydrolysis of the networks by lowering the concentration of water, the local environment around the hydrolyzable aryl ether bonds[44] in networks **2** and **3** may also inhibit hydrolysis. As a result, the decrease in glass transition temperature on exposure to water at elevated temperatures, a major concern for applications of polycyanurate networks, is mitigated as shown in Figure 8, which illustrates the measured "wet" T_G values measured by dynamic TMA (raw data in Supporting Information) compared to the dry T_G values predicted from the diBenedetto equation.[36] These dry T_G values are generated from the combined DSC/FTIR analysis for conversions described in the Supporting Information. It is important to note that *in situ* cure of the "wet" samples during analysis also takes place,[14] so that the "wet" network conversion during measurement (which is difficult to determine) is higher than the initial conversion of the as-prepared dry networks used to construct Figure 8.

Figure 8 clearly shows that while the "wet" T_G values for network **1** are lower than the dry values across the range of conversions studied, those for network **2** are nearly the same or slightly higher, while those for network **3** are higher at low
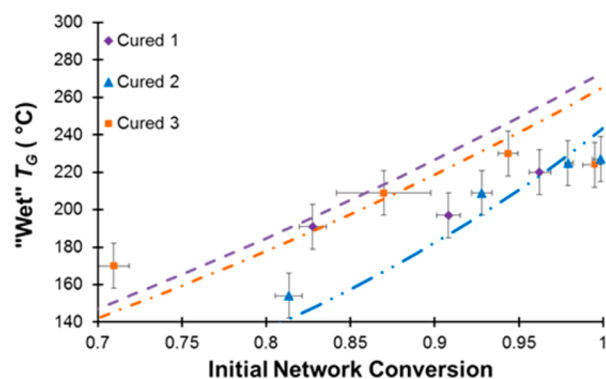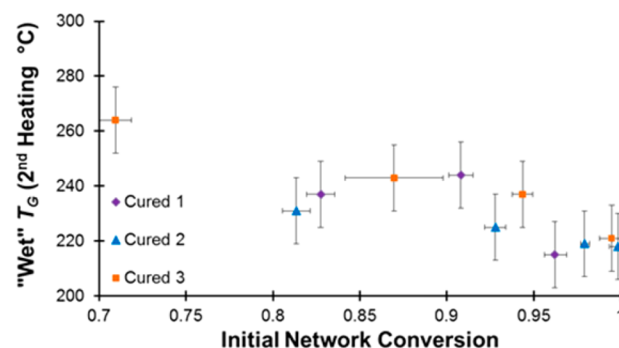
Figure 8. "Wet" glass transition temperature (after 96 h immersion in water at 85 °C). The diBenedetto equation fits of "dry" glass transition temperatures measured by DSC as a function of initial network conversion are indicated by the lines.

Figure 9. "Wet, fully-cured" glass transition temperature (after 96 h immersion in water at 85 °C, followed by heating to 350 °C at 20 °C/min).

conversions, but lower at high conversions. Comparison with Figure 6 shows that whenever water uptake is low and decreases slowly with increasing conversion, there is little hydrolysis, and the "wet" T_G tends to be a bit higher than the dry value due to *in situ* cure as discussed earlier. In contrast, whenever the water uptake increases significantly with increasing conversion, hydrolysis lowers the T_G of the "wet" network to a significant extent. A large increase in water uptake with increasing conversion is thought to signify a relatively "open" network structure in which cyanurates are accessible to water,[32] so it seems logical that under such circumstances hydrolysis would be enhanced. For applications, however, the absolute value of the "wet" T_G is often more important than the rate of hydrolysis, depending on exposure conditions. For the conditions tested, network **3** at about 95% conversion performs best because it combines a relatively high initial dry T_G with a more limited extent of hydrolysis. The higher dry T_G values may be attributed to the relatively bulky substitution around the bridge between aromatic rings in networks **1** and **3**. By combining the bulky substitution pattern that increases T_G values generally with a local environment that inhibits water uptake around the cyanurate oxygen, network **3** provides an optimized structure for high "wet" T_G values over a range of initial conversions from around 70−95%.

In addition to hydrolysis leading to the loss of cross-linking, water may also affect polycyanurate networks by converting reactive cyanate ester groups into carbamate groups, which then decompose with loss of CO_2 on heating above about 180 °C,[45] with the net effect being the conversion of cross-linkable chain ends into "loose" ends. Such a transformation lowers the T_G of the network at full cure. Measurements of the T_G of networks at full cure after exposure to water, accomplished by heating the "wet" networks to 350 °C, thus reveal information about the extent of both cross-link loss by hydrolysis (which also lowers the T_G) and carbamate formation. A complicating factor is that heating of the network to 350 °C even under dry conditions can lead to some degradation and concomitant loss in T_G.[46]

Figure 9 shows the measured T_G values for the "wet" samples after heating to 350 °C. From the DSC/FTIR analysis, the expected T_G values for fully cured, nondegraded networks are 274 °C for **1**, 244 °C for **2**, and 266 °C for **3**. None of the networks exhibit T_G values close to those expected for intact, fully cured networks, indicating that water exposure followed by heating to 350 °C induces significant loss of cross-link density. The T_G values are highest for **3**, slightly lower for **1**, and slightly

lower still for **2**, matching the pattern seen for samples exposed to water but not heated to 350 °C, indicating the water exposure is likely the main driver of the loss in cross-link density. Interestingly, networks with a lower initial conversion prior to exposure show the least loss in cross-link density. If carbamate formation were the main driver of loss in cross-link density, one would expect the opposite trend. Thus, cyanurate hydrolysis appears to be the main driver of loss in cross-link density.

One way to compare the extent of hydrolysis and carbamate formation in each network is to subtract the dry T_G measured in a DSC scan of an identical sample heated to 350 °C from the measured (by dynamic TMA) wet T_G of each sample after heating to 350 °C. This method effectively baselines each network to its maximum attainable T_G value taking into account thermochemical degradation during heating. This method is not perfect because sample sizes, thermal lag, and heating rates all differ between the two methods, so that the exposure histories are not truly identical except for the presence of water. Nonetheless, the results are quite informative, as shown in Figure 10.
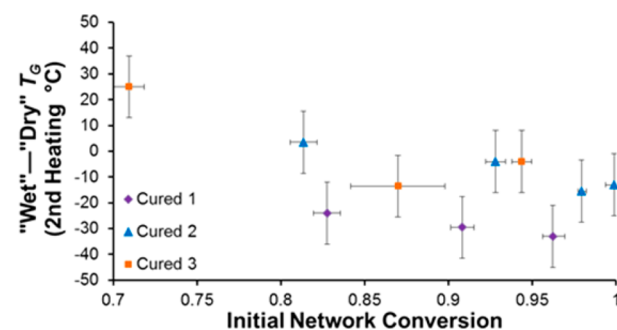

Figure 10. Difference between "wet" and "dry" glass transition temperature of fully cured single-component networks. This difference represents a relative measure of the amount of degradation induced by exposure to water at elevated temperature.

According to Figure 10, network **1** experiences the greatest loss in T_G due to exposure to water at elevated temperatures (20−40 °C), while networks **2** and **3** experience almost no loss and, in some cases, a net gain due to *in situ* cure of the "wet" samples during measurement. Extrapolating the trends to complete conversion eliminates both *in situ* cure effects as well as any differences in carbamate generation, resulting in one of the best comparative measures of the effect of network

structure on hydrolysis rate. By this measure, networks **2** and **3** are not significantly different; both are significantly better than network **1** at preventing hydrolysis despite the different local environments around the cyanurate oxygen atoms. Note also that the dependence of T_G loss on conversion is only about half as great as that seen in Figure 9, indicating that even "dry" samples with higher initial conversions end up with lower "fully cured" T_G values. The most likely explanation for this effect is that the higher cure temperatures required to generate the higher conversions lead to increased side reactions that destroy the reactive cyanate ester groups during cure. A more detailed analysis of these effects is provided in the Supporting Information.

Because the local environment that inhibits hydrolysis reactions is also present in the monomer, a potential negative consequence is increased difficulty in achieving complete cyclotrimerization of the networks. Once vitrification has taken place, it could be argued that issues such as steric hindrance at reactive sites take on less importance compared to the overall dynamics of diffusion within the network. One way to investigate these issues is to examine the observed network T_G as a function of cure temperature. Figure 11 shows
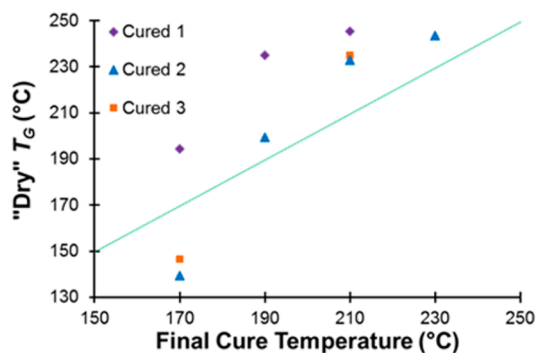

Figure 11. Observed dry glass transition temperature as a function of cure temperature (all samples cured for 24 h). The dotted line indicates the equivalence of the cure and glass transition temperatures. For data points above and to the left of this line, vitrification takes place during cure.

comparative T_G data for the networks used in this study. Network **1** consistently achieved the highest T_G values, even when (as at 170 °C) networks **2** and **3** did not vitrify during cure. The T_G values achieved for networks **2** and **3** were quite similar, despite the differences in monomer structure.

One shortcoming of Figure 11 is that it does not take into account different diBenedetto equation parameters for different networks. In particular, at high cure temperatures the T_G for each network will approach a separate maximum attainable value, while the conversion at which vitrification takes place is different for different networks cured at the same temperature. In Figure 12, the conversions achieved during cure are plotted as a function of the conversion at vitrification. Because conversion represents a "universal" scale for all networks, comparisons among networks are facilitated.

Using this representation, network **3** shows behavior that is intermediate between networks **1** and **2**. Network **1** consistently achieved conversions well beyond the vitrification point (a common occurrence for polycyanurate networks)[47,48] while network **2** failed to do so under identical cure and conversion conditions. These data indicate that the relatively higher conversions achieved in network **2** may result principally
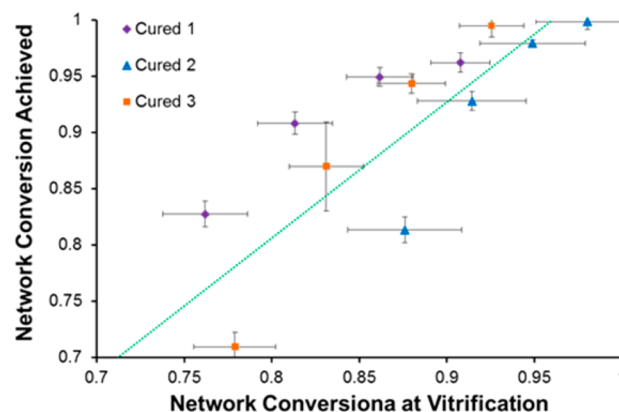
Figure 12. Extent of network conversion compared to the expected vitrification point (a measure of the ease of cure). The dotted line represents the expected result if cure were to cease completely upon vitrification, which is generally not the case for polycyanurates. Points further above and to the left of the line indicate a greater extent of cure after vitrification.

from lower glass transition temperatures at high conversions, which enabled these networks to avoid vitrification during cure. Methylation *ortho* to cyanate ester groups may therefore facilitate cure by lowering glass transition temperatures (avoiding vitrification), even though once vitrification takes place, these groups may hinder further cure. Of additional note, networks **2** and **3** achieved complete conversion at the highest cure temperature studied (230 °C), while network **1** did not (see the conversion data in the Supporting Information). This result may indicate that degradation during cure at elevated temperature (also discussed in the Supporting Information) is more pronounced in network **1**, while decreased degradation in networks **2** and **3** facilitates complete cure by enabling higher cure temperatures to be utilized without degradation.

A final stability consideration that is worthy of examination is the thermochemical stability of the cured network. Figure 13
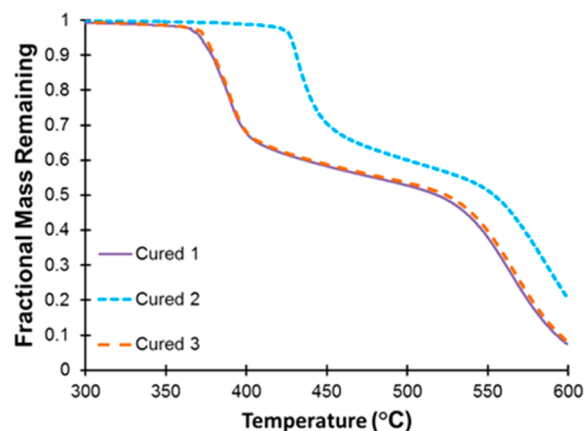
Figure 13. TGA mass loss traces in air. Note that all networks were cured at 230 °C for 24 h prior to the start of the TGA experiment.

shows TGA traces in air for each network. (A tabular summary of TGA data is provided in the Supporting Information.) Interestingly, networks **1** and **3** exhibit remarkably similar behavior, while network **2** appears to be significantly more stable. Figure 14 shows analogous TGA data under nitrogen, with a separately synthesized batch of network **2** added in order to assess the effect of variable trace impurities found during
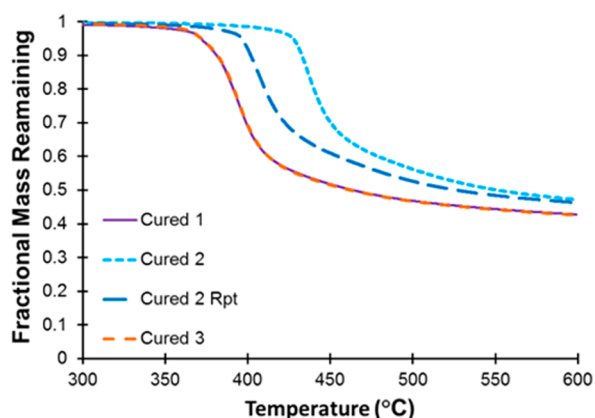
Figure 14. TGA mass loss traces under nitrogen, with a separately synthesized batch of network **2** added to assess reproducibility. Note that all networks were cured at 230 °C for 24 h prior to the start of the TGA experiment.

synthesis. Although the char yields do not change much between batches, the initial decomposition temperature (likely a reflection of decomposition kinetics)[49] does show substantial variation, indicating that as previously reported, impurities play a key role in thermochemical stability.[50] (The other physical properties and chemical analysis of the two batches of **2** were very similar, and the observed difference in the onset of degradation between the two batches of about 30 °C is many times larger than the estimated measurement error of 3−5 °C for this technique.[42])

If variability due to impurities is a significant factor in the thermochemical decomposition kinetics of polycyanurate networks, then the remarkable similarity in the decomposition behavior of networks **1** and **3** requires an explanation. The most interesting potential explanation is that because **1** and **3** are synthesized by the same reaction technique with the same starting materials, using only different separation procedures to isolate one product or the other, the same set of impurities is generated. Another potential explanation is that the *ortho*-methylation present in **2** inhibits a degradation pathway by a mechanism that does not involve steric effects, such as electronic induction. If the inhibited mechanism, which may even be accelerated in a *meta*-methylated network, is a characteristic of the network segments themselves, rather than impurities, it may be the rate-determining step, leading to consistent behavior. Only in its absence would mechanisms involving impurities become rate-determining. Examining the char yields in nitrogen, which are insensitive to kinetics, does show that network **2** performs consistently better than **1** or **3**, so that methylation *ortho* to cyanurate groups does lead to improved thermochemical stability, in at least one aspect, compared to networks with substitution *ortho* to the bridge linkage.

CONCLUSIONS

The configuration of network segments, primarily through various patterns of substitution on the phenyl rings, particularly near cyanurate oxygen atoms, has a substantial effect on the physical properties, cure properties, and stability of poly-cyanurate networks. These effects were illustrated via synthesis, network formation, and characterization of an isomeric series of *n*-propyl-bridged cyanate ester monomers. Substitution of aliphatic groups in a position *ortho*- to cyanurate oxygen

atoms, whether provided by methyl groups or aliphatic bridge groups, significantly lowered the moisture uptake of the networks and led to decreased loss in glass transition temperatures due to hydrolysis. In terms of absolute "wet" glass transition temperatures, however, the properties of *ortho,para*-linked aryl cyanates proved superior to *ortho*-methylated polycyanurate due to the fact that the former provides a higher dry glass transition temperatures of cured networks compared to the latter. Both forms of *ortho*-substitution still enabled the production of networks with >99% conversion at cure temperatures of 230 °C. Placement of methyl groups in an *ortho*-position, however, appeared to offer some benefits compared to placement of groups in the *meta*-position, even in systems with *ortho*-substitution provided by the bridge, with respect to thermochemical stability.

◼ ASSOCIATED CONTENT

Ⓢ Supporting Information
The Supporting Information is available free of charge on the ACS Publications website at DOI: 10.1021/acs.macro-mol.7b00824.

> NMR data (S1); comparison of properties of **1** with previously published data (S2); determination of conversions for networks, including DSC and FTIR data (S3); calculation of van der Waals volumes (S4); determination of key number density parameters for networks (S5); dynamic TMA data for "wet" samples (S6); examination of "fully cured" glass transition temperature data (S7); tabular summary of TGA data (S8); GC-MS parameters (S9) (PDF)

◼ AUTHOR INFORMATION

Corresponding Author
*E-mail andrew.guenthner@us.af.mil (A.J.G.).
ORCID Ⓞ
Andrew J. Guenthner: 0000-0002-6640-0176
Notes
The authors declare no competing financial interest.

◼ REFERENCES

(1) *Chemistry and Technology of Cyanate Ester Resins*, Hamerton, I., Ed.; Chapman & Hall: London, 1994.
(2) Fang, T.; Shimp, D. A. Polycyanate Esters − Science and Applications. *Prog. Polym. Sci.* **1995**, 20, 61−118.
(3) Nair, C. P. R.; Mathew, D.; Ninan, K. N. In *New Polymerization Techniques and Synthetic Methodologies*; Abe, A., Albertsson, A.-C., Cantow, H. J., Eds.; Springer-Verlag: Berlin, 2001; Vol. 155, pp 1−99.
(4) Hamerton, I.; Hay, J. N. Recent technological developments in cyanate ester resins. *High Perform. Polym.* **1998**, 10, 163−174.
(5) Arepalli, S.; Moloney, P. Engineered nanomaterials in aerospace. *MRS Bull.* **2015**, 40, 804−811.
(6) Dawson, D. Composites carry the Curiosity rover to a safe Mars landing *High Performance Composites*, May 2014; http://www.compositesworld.com/articles/composites-carry-the-curiosity-rover-to-a-safe-mars-landing, accessed 20 Nov 2016.
(7) Hill, J.; Munshi, N.; Tupper, M.; Babcock, H.; Kintz, A.; Kearns, T.; Kimoto, A. Risk Mitigation for Cyanate Ester Insulation of Large Magnets Through Cure Optimization. *IEEE Trans. Appl. Supercond.* **2015**, 25, 1−5.

(8) Humer, K.; Prokopec, R.; Weber, H. W.; Fillunger, H.; Maix, R. K. Characterization and Qualification of Advanced Insulators for Fusion Magnets. *Fusion Eng. Des.* **2013**, *88*, 350−360.

(9) Bittner-Rohrhofer, K.; Humer, K.; Fillunger, H.; Maix, R. K.; Weber, H. W.; Fabian, P. E.; Munshi, N. A. Radiation Effects on the Mechanical Integrity of Novel Organic Insulators for the ITER Magnet Coils. *J. Nucl. Mater.* **2004**, *329−333*, 1083−1087.

(10) Idesaki, A.; Nakamoto, T.; Yoshida, M.; Shimada, A.; Iio, M.; Sasaki, K.; Sugano, M.; Makida, Y.; Ogitsu, T. Development of high radiation-resistant glass fiber reinforced plastics with cyanate-based resin for superconducting magnet systems. *Fusion Eng. Des.* **2016**, *112*, 418−424.

(11) Fyfe, C. A.; Niu, J.; Rettig, S. J.; Burlinson, N. E. High-Resolution Carbon-13 and Nitrogen-15 NMR Investigations of the Mechanism of the Curing Reactions of Cyanate-Based Polymer Resins in Solution and the Solid State. *Macromolecules* **1992**, *25*, 6289−6301.

(12) Guenthner, A. J.; Reams, J. T.; Ford, M. D.; Lamison, K. R.; Mabry, J. M. In *Effect of in-Situ Cure on the Measurement of Glass Transition Temperatures in High-Temperature Thermosetting Polymers*; Society for the Advancement of Material and Process Engineering: 2015; SKU A-8568, 16 pp.

(13) Davis, M. C.; Guenthner, A. J.; Groshens, T. J.; Reams, J. T.; Mabry, J. M. Polycyanurate networks from anethole dimers: Synthesis and characterization. *J. Polym. Sci., Part A: Polym. Chem.* **2012**, *50*, 4127−4136.

(14) Davis, M. C.; Guenthner, A. J.; Sahagun, C. M.; Lamison, K. R.; Reams, J. T.; Mabry, J. M. Polycyanurate networks from dehydroanethole cyclotrimers: Synthesis and characterization. *Polymer* **2013**, *54*, 6902−6909.

(15) Cash, J. J.; Davis, M. C.; Ford, M. D.; Groshens, T. J.; Guenthner, A. J.; Harvey, B. G.; Lamison, K. R.; Mabry, J. M.; Meylemans, H. A.; Reams, J. T.; Sahagun, C. M. High Tg thermosetting resin from resveratrol. *Polym. Chem.* **2013**, *4*, 3859−3865.

(16) Cambrea, L. R.; Davis, M. C.; Garrison, M. D.; Groshens, T. J.; Lyon, R. E.; Safronava, N. Processable cyanate ester resin from *Cis* resveratrol. *J. Polym. Sci., Part A: Polym. Chem.* **2017**, *55*, 971−980.

(17) Harvey, B. G.; Sahagun, C. M.; Guenthner, A. J.; Groshens, T. J.; Cambrea, L. R.; Reams, J. T.; Mabry, J. M. A High-Performance Renewable Thermosetting Resin Derived from Eugenol. *ChemSusChem* **2014**, *7*, 1964−1969.

(18) Harvey, B. G.; Guenthner, A. J.; Yandek, G. R.; Cambrea, L. R.; Meylemans, H. A.; Baldwin, L. C.; Reams, J. T. Synthesis and characterization of a renewable cyanate ester/polycarbonate network derived from eugenol. *Polymer* **2014**, *55*, 5073−5079.

(19) Meylemans, H. A.; Harvey, B. G.; Reams, J. T.; Guenthner, A. J.; Cambrea, L. R.; Groshens, T. J.; Baldwin, L. C.; Garrison, M. D.; Mabry, J. M. Synthesis, Characterization, and Cure Chemistry of Renewable Bis(cyanate) Esters Derived from 2-Methoxy-4-Methylphenol. *Biomacromolecules* **2013**, *14*, 771−780.

(20) Harvey, B. G.; Guenthner, A. J.; Meylemans, H. A.; Haines, S. R. L.; Lamison, K. R.; Groshens, T. J.; Cambrea, L. R.; Davis, M. C.; Lai, W. W. Renewable thermosetting resins and thermoplastics from vanillin. *Green Chem.* **2015**, *17*, 1249−1258.

(21) Harvey, B. G.; Guenthner, A. J.; Koontz, T. A.; Storch, P. J.; Reams, J. T.; Groshens, T. J. Sustainable hydrophobic thermosetting resins and polycarbonates from turpentine. *Green Chem.* **2016**, *18*, 2416−2423.

(22) Laskoski, M.; Clarke, J. S.; Neal, A.; Harvey, B. G.; Ricks-Laskoski, H. L.; Hervey, W. J.; Daftary, M. N.; Shepherd, A. R.; Keller, T. M. Sustainable High-Temperature Phthalonitrile Resins Derived from Resveratrol and Dihydroresveratrol. *ChemistrySelect* **2016**, *1*, 3423−3427.

(23) Sharma, P.; Lochab, B.; Kumar, D.; Roy, P. K. Sustainable Bis-benzoxazines from Cardanol and PET-Derived Terephthalamides. *ACS Sustainable Chem. Eng.* **2016**, *4*, 1085−1093.

(24) Mehta, B.; Watt, P.; Soucek, M. D.; Pugh, C. Moderate Temperature Curing of Plant Oils with Bismaleimides via the Ene Reaction. *Ind. Eng. Chem. Res.* **2016**, *55*, 11727−11735.

(25) Puchot, L.; Verge, P.; Fouquet, T.; Vancaeyzeele, C.; Vidal, F.; Habibi, Y. Breaking the symmetry of dibenzoxazines: a paradigm to tailor the design of bio-based thermosets. *Green Chem.* **2016**, *18*, 3346−3353.

(26) Hannoda, Y.; Akasaka, Y.; Shibata, M. Bio-based thermosetting bismaleimide resins using cardany linolenate and allyl cardanyl ether. *React. Funct. Polym.* **2015**, *97*, 96−104.

(27) Shibata, M.; Shimasaki, T.; Satoh, H.; Iwai, M.; Neda, M. Bio-based thermosetting resins composed of aliphatic polyol-derived polymaleimides and allyleugenol. *React. Funct. Polym.* **2015**, *97*, 69−76.

(28) Shibata, M.; Tetramoto, N.; Imada, A.; Neda, M.; Sugimoto, S. Bio-based thermosetting bismaleimide resins using eugenol, bieugenol and eugenol novolac. *React. Funct. Polym.* **2013**, *73*, 1086−1095.

(29) Shibata, M.; Teramoto, N.; Nakamura, Y. High performance bio-based thermosetting resins composed of tung oil and bismaleimide. *J. Appl. Polym. Sci.* **2011**, *119*, 896−901.

(30) Hirayama, K.-I.; Irie, T.; Teramoto, N.; Shibata, M. High-performance bio-based thermosetting resins composed of dehydrated castor oil and bismaleimide. *J. Appl. Polym. Sci.* **2009**, *114*, 1033−1039.

(31) Harvey, B. G.; Guenthner, A. J.; Lai, W. W.; Meylemans, H. A.; Davis, M. C.; Cambrea, L. R.; Reams, J. T.; Lamison, K. R. Effects of o-Methoxy Groups on the Properties and Thermal Stability of Renewable High-Temperature Cyanate Ester Resins. *Macromolecules* **2015**, *48*, 3173−3179.

(32) Guenthner, A. J.; Wright, M. E.; Chafin, A. P.; Reams, J. T.; Lamison, K. R.; Ford, M. D.; Kirby, S. P. J.; Zavala, J. J.; Mabry, J. M. Mechanisms of Decreased Moisture Uptake in ortho-Methylated Di(Cyanate Ester) Networks. *Macromolecules* **2014**, *47*, 7691−7700.

(33) Shimp, D. A. The translation of dicyanate structure and cyclotrimerization efficiency to polycyanurate properties. *Polym. Mater. Sci. Eng.* **1986**, *54*, 107−113.

(34) Harden, W. C.; Reid, E. E. Condensation of certain phenols with some aliphatic anhydrides. *J. Am. Chem. Soc.* **1932**, *54*, 4325−4334.

(35) Gómez, C. M.; Recalde, I. B.; Mondragon, M. Kinetic parameters of a cyanate ester resin catalyzed with different proportions of nonylphenol and cobalt acetylacetonate catalyst. *Eur. Polym. J.* **2005**, *41*, 2734−2741.

(36) Pascault, J. P.; Williams, R. J. J. Glass transition temperature versus conversion relationships for thermosetting polymers. *J. Polym. Sci., Part B: Polym. Phys.* **1990**, *28*, 85−95.

(37) Reams, J. T.; Guenthner, A. J.; Lamison, K. R.; Vij, V.; Lubin, L. M.; Mabry, J. M. Effect of Chemical Structure and Network Formation on Physical Properties of Di(Cyanate Ester) Thermosets. *ACS Appl. Mater. Interfaces* **2012**, *4*, 527−535.

(38) Georjon, O.; Galy, J. Effects of crosslink density on the volumetric properties of high Tg polycyanurate networks. Consequences on moisture absorption. *Polymer* **1998**, *39*, 339−345.

(39) Guenthner, A. J.; Sahagun, C. M.; Lamison, K. R.; Reams, J. T.; Haddad, T. S.; Mabry, J. M. Effect of Nanoparticle Functionalization on the Performance of Polycyanurate/Silica Nanocomposites. *Ind. Eng. Chem. Res.* **2016**, *55*, 7096−7107.

(40) Hay, J. N. Processing and cure schedules for cyanate ester resins. In *Chemistry and Technology of Cyanate Ester Resins*; Hamerton, I., Ed.; Chapman & Hall: London, 1994; pp 165−166.

(41) Bicerano, J. *Prediction of Polymer Properties*, 3rd ed.; Marcel Dekker, Inc.: New York, 2002; pp 66−78.

(42) Guenthner, A. J.; Lamison, K. R.; Vij, V.; Reams, J. T.; Yandek, G. R.; Mabry, J. M. New Insights into Structure-Property Relationships in Thermosetting Polymers from Studies of Cocured Polycyanurate Networks. *Macromolecules* **2012**, *45*, 211−220.

(43) See: Simon, S. L.; Gillham, J. K. Cure kinetics of a thermosetting liquid dicyanate ester monomer/high Tg polycyanurate material. *J. Appl. Polym. Sci.* **1993**, *47*, 461−485. Note that the glass transition temperature of RTX-366 at full cure of 190 °C is much lower than typical polycyanurates, while the moisture uptake as listed in *Chemistry and Technology of Cyanate Ester Resins*, Hamerton, I., Ed.; Chapman & Hall: London, 1994; p 332 is also quite low at 0.6%.

(44) Kasehagen, L. J.; Haury, I.; Macosko, C. W.; Shimp, D. A. Hydrolysis and blistering of cyanate ester networks. *J. Appl. Polym. Sci.* **1997**, *64*, 107−113.

(45) Shimp, D. A.; Ising, S. J. Moisture effects and their control in the curing of polycyanate resins. *Polym. Mater. Sci. Eng.* **1992**, *66*, 504−505.

(46) Georjon, O.; Galy, J.; Pascault, J. P. Isothermal Curing of an Uncatalyzed Dicyanate Ester Monomer: Kinetics and Modeling. *J. Appl. Polym. Sci.* **1993**, *49*, 1441−1452.

(47) Guenthner, A. J.; Davis, M. C.; Ford, M. D.; Reams, J. T.; Groshens, T. J.; Baldwin, L. C.; Lubin, L. M.; Mabry, J. M. Polycyanurate Networks with Enhanced Segmental Flexibility and Outstanding Thermochemical Stability. *Macromolecules* **2012**, *45*, 9707−9718.

(48) Mondragon, I.; Solar, L.; Recalde, I. B.; Gómez, C. M. Cure kinetics of a cobalt catalysed dicyanate ester monomer in air and argon atmospheres from DSC data. *Thermochim. Acta* **2004**, *417*, 19−26.

(49) Guenthner, A. J.; Reams, J. T.; Lamison, K. R.; Ramirez, S. M.; Swanson, D. D.; Yandek, G. R.; Sahagun, C. M.; Davis, M. C.; Mabry, J. M. Synergistic Physical Properties of Cocured Networks Formed from Di- and Tricyanate Esters. *ACS Appl. Mater. Interfaces* **2013**, *5*, 8772−8783.

(50) Hamerton, I. Properties of unreinforced cyanate ester matrix resins. In *Chemistry and Technology of Cyanate Ester Resins*; Hamerton, I., Ed.; Chapman & Hall: London, 1994; pp 193−229.